Journal of Computational Physics **179,** 349–370 (2002)
doi:10.1006/jcph.2001.6798

A Novel Gauge Invariant Multistate Smearing Technique

P. Boyle[1]

Department of Physics and Astronomy, University of Edinburgh, Edinburgh
UKQCD Collaboration
E-mail: pboyle@physics.gla.ac.uk

Received March 29, 2000; revised March 26, 2001

We present an investigation of a gauge invariant smearing technique that allows the construction of smearing functions with arbitrary radial behavior, by foresaking the space-filling nature of traditional smearing techniques. This is applied to both heavy–heavy, heavy–light, and light–light systems with one particular choice of radial "wavefunction"—the hydrogenic solutions—and we find good stability for both fitted masses and amplitudes of the radially excited states. The dependence of the amplitudes on the smearing radius is demonstrated to be well understood, while near optimal smearing radii may be found with extremely low statistics using a property of the smeared-local correlator. The smearing technique is inexpensive since it is noniterative, achieves a good signal-to-noise ratio, and can be altered to use wavefunctions from, say, potential models or the Bethe–Salpether equations in future simulations.

I. INTRODUCTION

Smearing is a technique that has been used for some time in Lattice QCD simulations [1–3] in order to improve the quality of the results obtained for a given computational expense by reducing the extent of excited state contamination. The choice of operator used to represent a state in any given simulation is essentially free within the constraint that it must have the appropriate quantum numbers of the desired state, which (usually) guarantees nonzero overlap with the groundstate of those quantum numbers. In Euclidean space, all such operators asymptotically behave as the lowest lying state with quantum numbers matching those of the operator.[2] We consider the two-point correlation function of a set of operators

[1] Present address: Department of Physics and Astronomy, University of Glasgow, Glasgow.

[2] Ignoring questions such as scalar glueball mixing in quenched simulations, and as we shall see special cases where the overlap is fine tuned to be near zero.

0021-9991/02 $35.00

TABLE I
Smearing combinations

κ_1	Source	Sink	κ_2	Source	Sink
2300	L	L	2300	L	L
2300	L	F	2300	L	L
2300	R_{10}	L	2300	L	L
2300	R_{10}	L	2300	R_{10}	L
2300	R_{10}	R_{10}	2300	L	L
2300	L	R_{20}	2300	L	L
2300	R_{10}	R_{20}	2300	R_{10}	L
2300	L	L	3460	L	L
2300	L	F	3460	L	L
2300	R_{10}	L	3460	L	L
2300	R_{10}	R_{10}	3460	L	L
2300	L	R_{10}	3460	L	L
2300	L	R_{20}	3460	L	L
3460	L	L	3460	L	L
3460	L	F	3460	L	L
3460	L	R_{20}	3460	L	L
3460	L	R_{10}	3460	L	L
3460	L	R_{10}	3460	L	R_{10}

$\mathcal{O}_k$ with some definite J^{PC} in a Euclidean lattice of temporal extent T. When we insert a complete set of physical intermediate states of the same quantum numbers, we find the same asymptotic behavior for all operators

$$\langle \mathcal{O}_k(x)\mathcal{O}_k^\dagger(0)\rangle = \sum_n \frac{\langle 0|\mathcal{O}_k|n\rangle\langle n|\mathcal{O}_k^\dagger|0\rangle}{2E_n} e^{-E_n\frac{T}{2}} \cosh E_n\left(t-\frac{T}{2}\right) \tag{1}$$

$$= \sum_n C_{kn}C_{kn}^* \frac{e^{-E_n\frac{T}{2}}}{2E_n} \cosh E_n\left(t-\frac{T}{2}\right) \tag{2}$$

$$\stackrel{t\to\infty}{\longrightarrow} |C_{k0}|^2 \frac{e^{-E_n\frac{T}{2}}}{2E_0} \cosh E_0\left(t-\frac{T}{2}\right). \tag{3}$$

This somewhat egalitarian situation is the principal reason why lattice calculations have traditionally had difficulty extending their scope to radially excited states. However, some choices of operators turn out to be more equal than others, depending on the relative values of the C_{nk}. For ground state phenomenology, we would like $C_{0k} \gg C_{nk}\,\forall n \geq 1$. To this end it is common to construct extended operators which project more predominantly onto the groundstate of the desired system; it is this extension procedure that has been dubbed smearing. Typically we require that the smearing procedure be parity and charge positive, and possess at least cubic symmetry.

There are two different schools of thought on how to construct smeared operators: gauge invariant smearing and gauge fixed smearing.

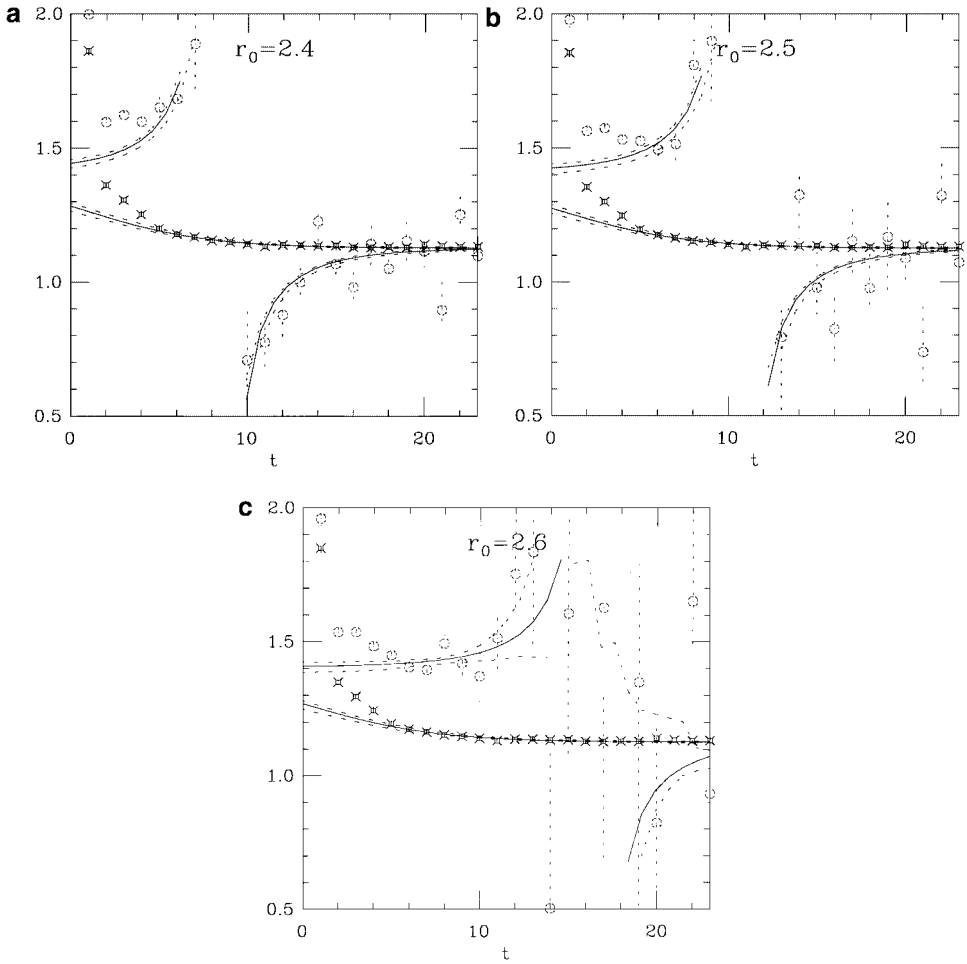

FIG. 1. Heavy–heavy pseudoscalar fits for $r_0 = 2.4, 2.5, 2.6$. The plots contain the effective masses in lattice units for correlators with R_{20} (circles) and R_{10} (fancy squares) source smearings with local sinks. The fits are simultaneous double exponential over the timeslice range 4–20. A clear transition between a pole in the R_{20} effective mass and a continuous effective mass is seen as r_0 is tuned across its optimal value.

A. *Gauge Invariant Smearing*

Explicit gauge invariance is one of the most attractive features of nonperturbative simulation techniques, and remains to this day a necessary (but sadly insufficient) condition for correct operation of simulation code. Further, the gauge fixing process may be multiply defined because of Gribov ambiguities of some gauge fixing conditions [4, 5], and one has to assume that the ambiguity does not cause any bias in the quantities being measured. For these reason, many people are unwilling to use gauge fixing, and therefore proceed with one of a number of gauge invariant techniques.

The most commonly used gauge invariant techniques are Wuppertal [1], Jacobi [2, 6], and Fuzzed [3] smearing. Wuppertal smearing covariantly smears the quark fields with a spatial distribution which is the solution of the scalar Klein Gordon equation on a given gauge configuration, while Jacobi smearing is a numerically efficient way to approximate this. In order to preserve gauge invariance, both of the first two methods iteratively apply a

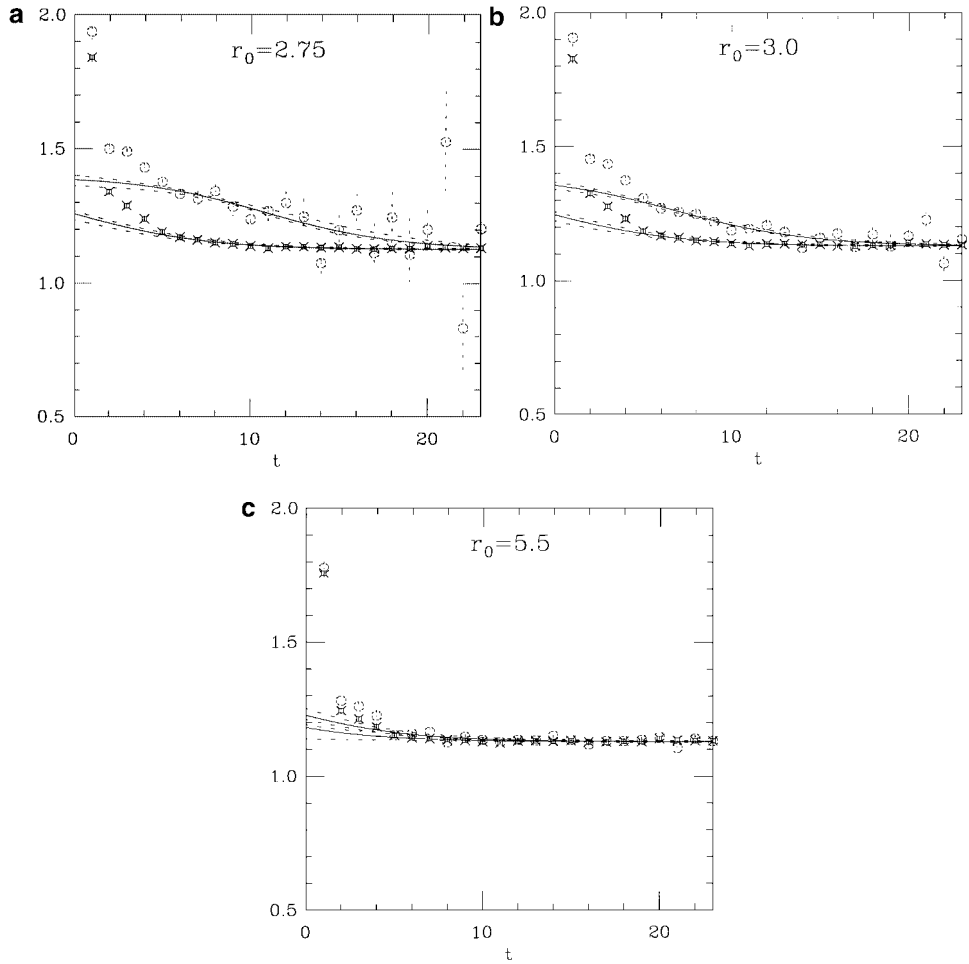

FIG. 2. Heavy–heavy pseudoscalar fits $r_0 = 2.75, 3.0, 5.5$. The plots contain the effective masses in lattice units for correlators with R_{20} (circles) and R_{10} (fancy squares) source smearings with local sinks. The fits are simultaneous double exponential over the timeslice range 4–20.

gauge invariant nearest neighbor operator to smear out a quark field, with limiting behavior to weight sites in a "bell shaped" distribution. Given the extended nature of the physical states, and the wavefunction picture in the nonrelativistic limit, one would expect smeared operators to more accurately project onto the ground state, and indeed this is borne out by simulations. However, these gauge invariant techniques give little control over the precise functional form of the smearing beyond a basic radius parameter.

The cost of iteratively applying, say, the Jacobi operator N times on a propagator is somewhat prohibitive. Lacock and Michael [3] suggested the use of a covariantly transported "cross" using low noise *fuzzed* links. The fuzzing prescription iterates

$$U'_j(x) = cU_j(x) + \sum_{i \neq j} \left[U_i^{\text{Staple}}(x, x+\hat{j}) + U_{-i}^{\text{Staple}}(x, x+\hat{j}) \right], \tag{4}$$

$$U_j(x) = \mathcal{P}\, U'_j(x), \tag{5}$$

where $\mathcal{P}$ is a projection onto SU(3) (not closed under addition) by Cabibbo Marinari

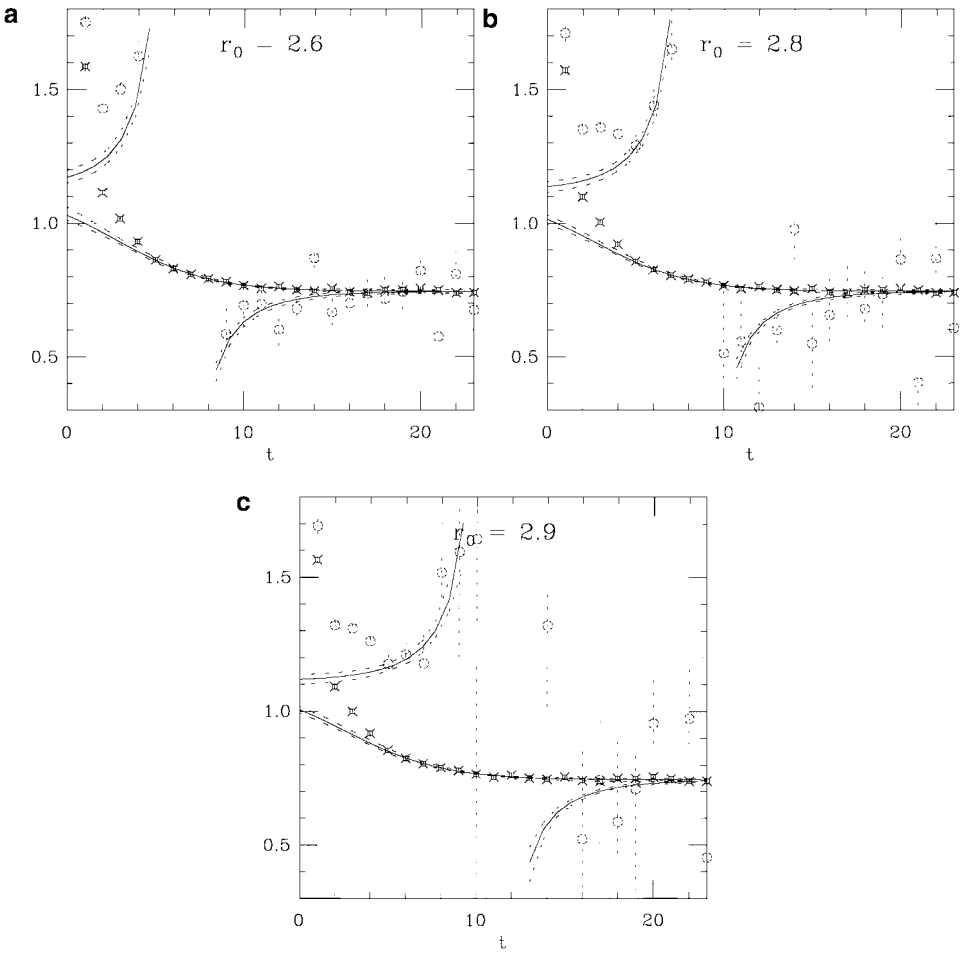

FIG. 3. Heavy–light pseudoscalar fits, $r_0 = 2.6, 2.8, 2.9$. The plots contain the effective masses in lattice units for correlators with R_{20} (circles) and R_{10} (fancy squares) source smearings with local sinks. The fits are simultaneous double exponential over the timeslice range 4–20.

maximization of $\mathrm{Tr}[U_j^\dagger U_j']$ with six hits on each SU(2) subgroup. Typically, c is set to 2.0, and there are five iterations performed. These fuzzed links are used to transport the quark field by some number of sites N along each of the spatial axes,

$$\psi'(x) = \sum_{i=x,y,z} \left[\prod_{n=1}^{r} U_i(x + (n-1)\hat{i})\right] \times \psi(x + r\hat{i}) + \left[\prod_{n=1}^{r} U_i^\dagger(x - n\hat{i})\right] \times \psi(x - r\hat{i}). \quad (6)$$

The fuzzing radius, r, is chosen to minimize the contamination of the ground state operator.

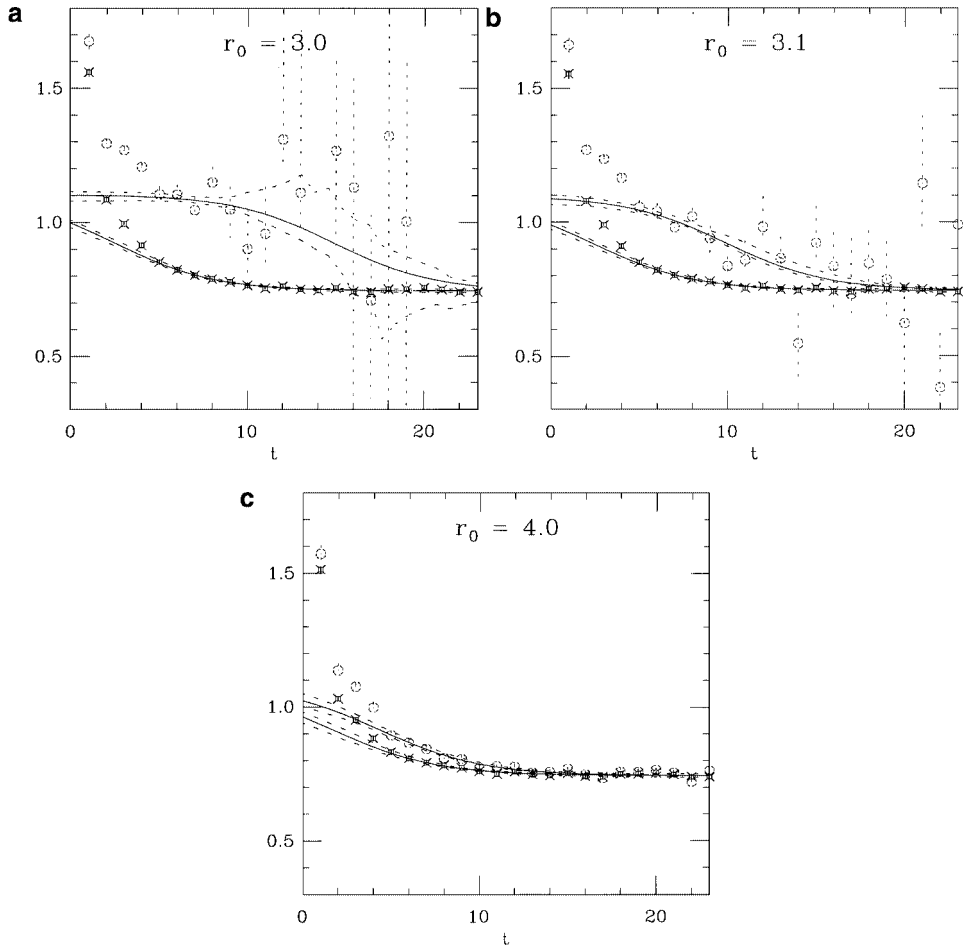

FIG. 4. Heavy–light pseudoscalar fits $r_0 = 3.0, 3.1, 4.0$. The plots contain the effective masses in lattice units for correlators with R_{20} (circles) and R_{10} (fancy squares) source smearings with local sinks. The fits are simultaneous double exponential over the timeslice range 4–20.

B. *Gauge Fixed Smearing*

Gauge fixed smearing (either Coulomb or Landau gauge) allows complete freedom for the functional form of the smearing; in a fixed gauge we are freed from the need to iterate local covariant transport to space fill, and convolve quark fields with arbitrary smearing functions using fast Fourier transforms. In particular, the use of smearing functions with nodes has allowed reliable extraction of excited state energies from NRQCD through the use of multi-exponential fits [7]. Neither the cost of Fourier transforming the data set multiple times to implement this smearing on a massively parallel machine nor the loss of gauge invariance are desirable features. There is clearly a need for a gauge invariant smearing technique with free radial functional form.

In order to proceed, we consider the nonrelativistic interpretation of $q\bar{q}$ systems in terms of spatial wavefunctions. This is certainly appropriate to heavy–heavy mesons, however, we can apply this technique in heavy–light and light–light systems without needing to worry about its relevance.

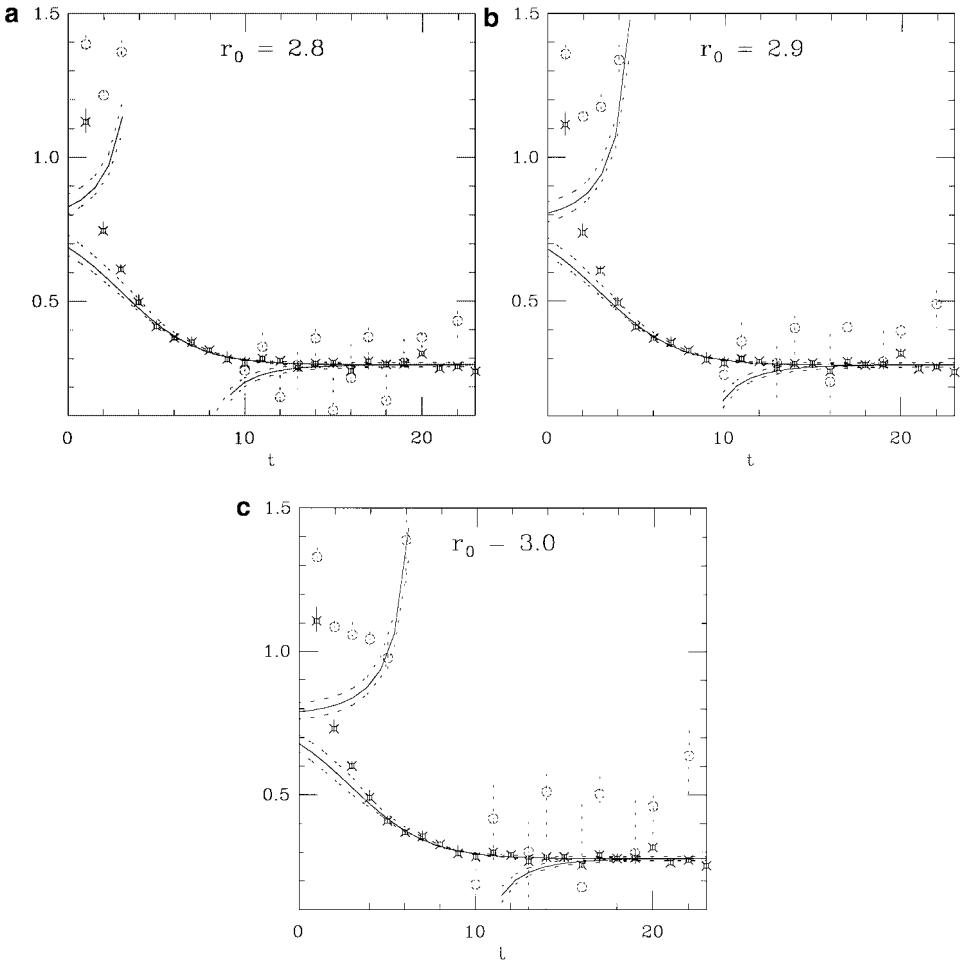

FIG. 5. Light–light pseudoscalar fits, $r_0 = 2.8, 2.9, 3.0$. The plots contain the effective masses in lattice units for correlators with R_{20} (circles) and R_{10} (fancy squares) sink smearings with local sources. The fits are simultaneous double exponential over the timeslice range 4–18.

II. SMEARING IN A NONRELATIVISTIC POTENTIAL

We consider smearing in the context of a nonrelativistic potential model with spherical symmetry. The solutions may be written as $\psi_{nlm}(r, \theta, \phi) = R_{nl}(r) P_{lm}(\theta, \phi)$ where $P_{lm}(\theta, \phi)$ are the usual spherical harmonics. The orthogonality relation of the wavefunctions is then

$$\int dV \psi^*_{mko} \psi_{nlp} = \delta_{kl} \delta_{op} \int_{r=0}^{\infty} R^*_{ml}(r) R_{nl}(r) r^2 \, dr \tag{7}$$

$$\Rightarrow \int_{r=0}^{\infty} R^*_{ml}(r) R_{nl}(r) r^2 \, dr = \delta_{mn}. \tag{8}$$

We shall ignore the l and m indices from here, and consider spherically symmetric functions. Suppose we construct nonlocal meson operators

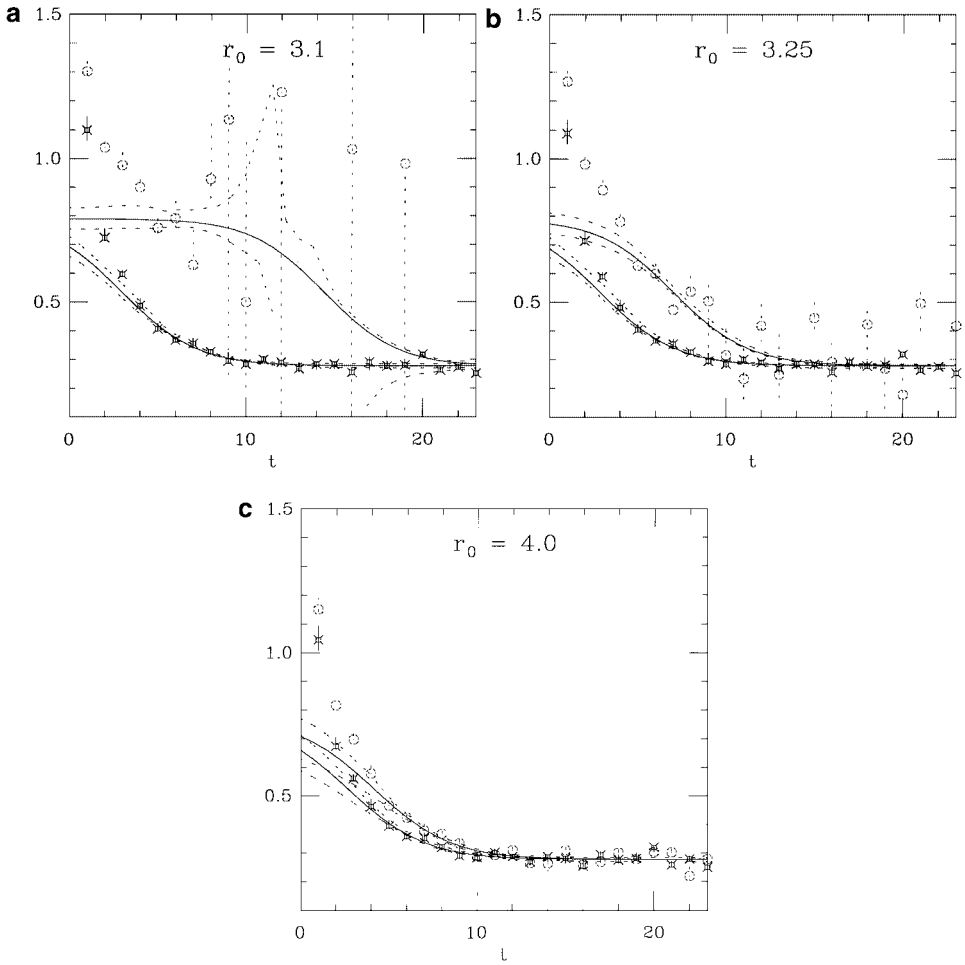

FIG. 6. Light–light pseudoscalar fits $r_0 = 3.1, 3.25, 4.0$. The plots contain the effective masses in lattice units for correlators with R_{20} (circles) and R_{10} (fancy squares) sink smearings with local sources. The fits are simultaneous double exponential over the timeslice range 4–18.

$$\mathcal{O}_n(x) = \int d^3y \bar{\psi}(y) S_n(y, x) \psi(x), \tag{9}$$

where the smearing function $S_n(y, x) = S_n(y - x)$ is thought of as a spatial wavefunction defined on lattice sites

$$S_n(y, 0) \equiv S_n(y) \sum_{i,j,k} \delta^3(y - i\hat{x} - j\hat{y} - k\hat{z}). \tag{10}$$

Note we have dropped the color indices since in our wavefunction approximation the gauge degrees of freedom are represented by a color singlet potential.

The operator $\mathcal{O}$ will have an overlap with each physical state $|\psi_m\rangle$ of the relevant J^{PC}

$$C_{nm} = \int \psi_m^*(x) S_n(x)\, dV = \sum_{i,j,k} \psi_m^*(i\hat{x} + j\hat{y} + k\hat{z}) S_n(i\hat{x} + j\hat{y} + k\hat{z}). \tag{11}$$

Now if $S_n(x)$ is chosen to well approximate the state $\psi_n(x)$ and the lattice is sufficiently fine that the sum (11) is close to the integral

$$C_{nm} = \int \psi_m^* S_n(x)\, dV \simeq \int \psi_m^*(x)\psi_n(x)\, dV = \delta_{nm}. \tag{12}$$

Thus, with a well-chosen set of smearing functions S_n, we can write

$$C_{nm} = \delta_{nm} + \eta_{nm}, \tag{13}$$

where η_{nm} is a small contamination to the signal, giving a set of correlation functions corresponding to each of the physical radial excitations. In fact, $\eta_{nm} \simeq 0 \quad \forall m < n$ guarantees that the lowest state significantly contributing to the correlation function of the nth radially excited operator is in fact the nth state, and the effective mass will not decay to the ground state of the J^{PC} on a finite lattice.

If we choose a nonspace-filling smearing function of the form

$$S_n(\vec{x}, 0) \equiv \sum_{r=0}^{N} r^2 \phi_n(r) \sum_{\hat{\mu}=\hat{x},\hat{y},\hat{z}} (\delta^3(\vec{x} - r\hat{\mu}) + \delta^3(\vec{x} + r\hat{\mu})), \tag{14}$$

where ϕ_n is some arbitrary modulating function that is chosen to approximate the true solution ψ_n, and the factor r^2 compensates for the nonspace-filling nature of the smearing, then the overlap is

$$C_{nm} = \int \psi_m^*(\vec{x}) S_n(\vec{x}, 0)\, dV \tag{15}$$

$$= \sum_{r=0}^{N} r^2 \phi_n(r) \psi_m^*(r) \tag{16}$$

$$\overset{a\to 0}{\to} \int_{r=0}^{\infty} r^2 \psi_m^* \phi_n\, dr \tag{17}$$

$$\simeq \delta_{nm}. \tag{18}$$

Thus, if we choose the ϕ_m correctly (i.e., to be ψ_n), then we establish the orthogonality relation required without the need for space filling. The new smearing technique proposed is a generalization of the above form to incorporate color,

$$\psi(x) \to \sum_{r=0}^{N} \left(r + \frac{1}{2}\right)^2 \phi_n(r) \sum_{i=x,y,z} \left\{ \left[\prod_{n=1}^{r} U_i(x + (n-1)\hat{i}) \right] \psi(x + r\hat{i}) + \left[\prod_{n=1}^{r} U_i^\dagger(x - n\hat{i}) \right] \psi(x - r\hat{i}) \right\}, \tag{19}$$

where the links are fuzzed links (c.f. Section IA). We use the factor $(r + \frac{1}{2})^2$ as opposed to r^2 so that there is a nonzero contribution from the local current, since this was observed to improve the statistical noise. The procedure is very similar in cost to fuzzing with a radius N, since all the terms can be formed as part of the process of fuzzing to the largest radius. The

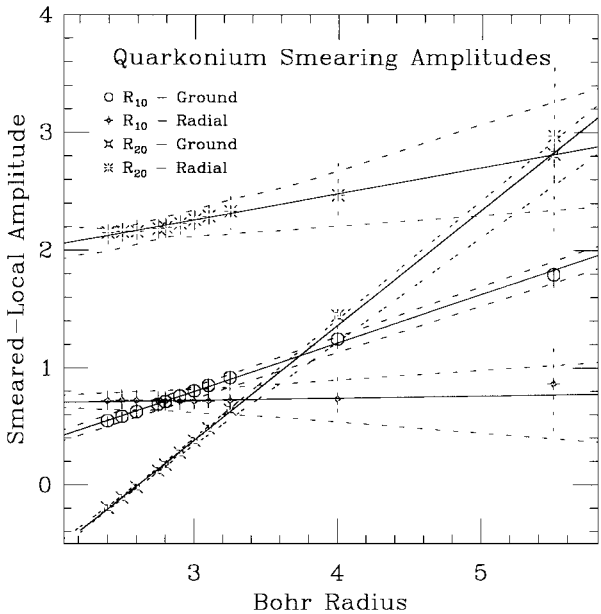

FIG. 7. Fitted amplitudes for quarkonia correlation functions using the timeslice range 4–20. The contaminating amplitude in the R_{20} source smeared correlator clearly shows a zero at $r_0 \simeq 2.6$.

technique therefore eliminates the two main problems with implementing gauge-invariant multistate smearing, namely that gauge invariance requires expensive iterative space-filling techniques, and that it restricts the functional form. Here we have a low-cost gauge invariant technique with an arbitrary functional form, allowing the insertion of both ground and radially excited wavefunctions.

We shall consider the case in which the physical solutions are approximately hydrogenic wavefunctions.

III. OPTIMIZING THE SMEARING

We consider the correlation function with a smeared source denoted R and a local sink denoted L, and restrict the argument to one contaminating excited state, and ignore the periodicity of the lattice

$$C_t = Ae^{-E_1 t} + Be^{-E_2 t}, \tag{20}$$

where $A \propto C_{L1}C^*_{R1}$ and $B \propto C_{L2}C^*_{R2}$. The effective mass of this correlator is loosely the negative of the derivative of the log:

$$M_t \simeq -\frac{d}{dt}\log C_t = \frac{E_1 + \frac{B}{A}E_2 e^{-(E_2-E_1)t}}{1 + \frac{B}{A}e^{-(E_2-E_1)t}}. \tag{21}$$

By inspection it can be seen that there are two distinct cases for the approach to the plateau:

TABLE II
Heavy Heavy Double Exponential Fit
Stability; $r_0 = 2.6$, $T_{max} = 20$

tmin	χ^2/dof	χ^2	Pseudo	Pseudo′
2	0.66	21.	1.123 (3)	1.45 (2)
3	0.25	7.5	1.125 (4)	1.42 (1)
4	0.13	3.7	1.127 (4)	1.41 (2)
5	0.13	3.3	1.128 (4)	1.40 (3)
6	0.13	3.2	1.129 (4)	1.40 (3)
7	0.14	3.1	1.130 (5)	1.40 (4)

TABLE III
Heavy Heavy Triple Exponential Fit Stability; $r_0 = 2.6$, $T_{max} = 20$

tmin	χ^2/dof	χ^2	Pseudo (2300,2300)	Pseudo′	Pseudo″
2	0.081	3.6	1.128 (4)	1.39 (3)	2.13 (4)
3	0.083	3.5	1.129 (5)	1.39 (3)	2.10 (10)
4	0.086	3.3	1.130 (6)	1.39 (4)	1.9 (2)
5	0.089	3.2	1.130 (5)	1.40 (7)	1.9 (2)
6	0.095	3.1	1.131 (6)	1.39 (8)	1.8 (2)

TABLE IV
Heavy Light Double Exponential Fit
Stability; $r_0 = 3.0$, $T_{max} = 20$

tmin	χ^2/dof	χ^2	Pseudo	Pseudo′
2	0.44	14.	0.746 (5)	1.18 (2)
3	0.15	4.5	0.745 (6)	1.13 (2)
4	0.074	2.1	0.744 (6)	1.10 (2)
5	0.076	2.0	0.744 (7)	1.09 (3)
6	0.078	1.9	0.744 (7)	1.08 (4)
7	0.083	1.8	0.744 (7)	1.07 (6)

TABLE V
Light Light Double Exponential Fit
Stability; $r_0 = 3.1$, $T_{max} = 18$

tmin	χ^2/dof	χ^2	Pseudo	Pseudo′
2	0.18	5.0	0.280 (7)	0.86 (4)
3	0.085	2.2	0.279 (7)	0.81 (3)
4	0.079	1.9	0.278 (7)	0.79 (4)
5	0.082	1.8	0.278 (7)	0.81 (6)

TABLE VI
Heavy Heavy Double Exponential Fit Stability with Bohr Radius

Bohr	tmin	χ^2/dof	χ^2	Pseudo	Pseudo′
2.60	4	0.13	3.7	1.127 (4)	1.41 (2)
2.75	4	0.083	2.3	1.128 (4)	1.40 (2)
2.80	4	0.066	1.9	1.128 (4)	1.40 (2)
2.90	4	0.045	1.2	1.128 (4)	1.39 (2)
3.00	4	0.033	0.92	1.128 (4)	1.39 (2)
3.10	4	0.026	0.74	1.128 (4)	1.39 (1)
3.25	4	0.021	0.59	1.128 (4)	1.39 (1)
4.00	4	0.016	0.44	1.128 (3)	1.39 (1)
5.50	4	0.016	0.44	1.129 (3)	1.40 (6)

TABLE VII
Heavy Light Double Exponential Fit Stability with Bohr Radius

Bohr	tmin	χ^2/dof	χ^2	Pseudo	Pseudo′
2.60	4	0.059	1.6	0.745 (6)	1.13 (3)
2.75	4	0.10	2.8	0.745 (6)	1.12 (2)
2.80	4	0.12	3.2	0.745 (6)	1.12 (2)
2.90	4	0.12	3.3	0.744 (6)	1.11 (2)
3.00	4	0.074	2.1	0.744 (6)	1.10 (2)
3.10	4	0.045	1.2	0.744 (6)	1.10 (2)
3.25	4	0.026	0.72	0.744 (6)	1.09 (2)
4.00	4	0.013	0.35	0.744 (6)	1.09 (3)
5.50	4	0.014	0.38	0.745 (6)	1.10 (5)

TABLE VIII
Light Light Double Exponential Fit Stability with Bohr Radius

Bohr	tmin	χ^2/dof	χ^2	Pseudo	Pseudo′
2.60	4	0.0053	0.13	0.278 (7)	0.79 (4)
2.75	4	0.010	0.24	0.278 (7)	0.78 (4)
2.80	4	0.013	0.32	0.278 (7)	0.78 (4)
2.90	4	0.029	0.70	0.278 (7)	0.78 (4)
3.00	4	0.077	1.9	0.278 (7)	0.78 (3)
3.10	4	0.079	1.9	0.278 (7)	0.79 (4)
3.25	4	0.023	0.55	0.278 (7)	0.79 (4)
4.00	4	0.0013	0.031	0.277 (6)	0.77 (7)
5.50	4	0.00072	0.017	0.277 (6)	0.8 (1)

- $\frac{B}{A} > 0$, approach from above, and
- $\frac{B}{A} < 0$, approach from below, vertical asymptote at $t = \frac{\log|\frac{B}{A}|}{E_2 - E_1}$.

Suppose the physical wave functions are well described by the hydrogenic wavefunctions, ψ_n, with some Bohr radius, r_1. We wish to approximate these solutions with a trial wavefunction, which we choose to be the hydrogenic solutions ϕ_m with Bohr radius r_2. Consider the overlap of the trial excited state with the physical groundstate,

$$C_{10} = \int r^2 \psi_0 \phi_1 \, dr \tag{22}$$

$$\propto \int r^2 \left(1 - \frac{r}{2r_2}\right) e^{-\frac{r}{2r_2}} e^{-\frac{r}{r_1}} \, dr \tag{23}$$

$$= c^3 \left[\Gamma(3) - \frac{c}{2r_2}\Gamma(4)\right] \tag{24}$$

$$\simeq 2c^4 \frac{\delta}{r_2^2}, \tag{25}$$

where $c = \frac{2r_1 r_2}{r_1 + 2r_2}$, $\delta = r_2 - r_1$, and the last step is made for small δ. Thus, the overlap of the excited state smearing with the physical state is proportional to the error in the Bohr radius. The overlap is positive for smearing radii that are too large, and negative for radii that are too small. Therefore the effective mass of the smeared–local correlation function will have a vertical asymptote for radii that are too small, and a smooth form for radii that are too large. This dramatic change of behavior may be used to tune the Bohr radius on very small statistical samples.

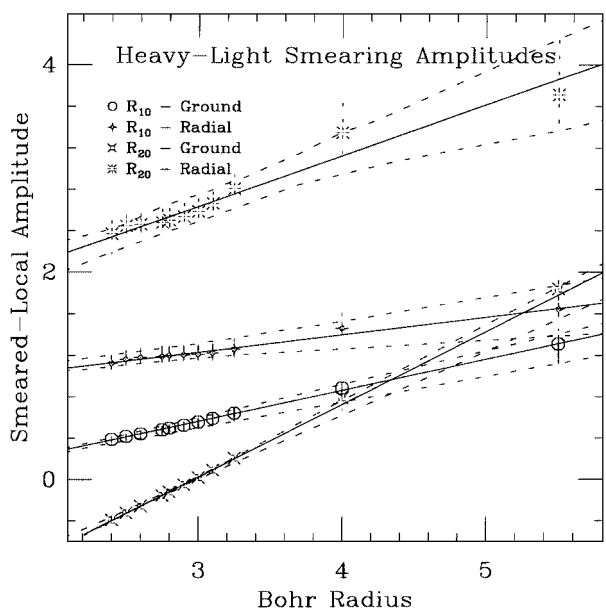

FIG. 8. Fitted amplitudes for heavy–light correlation functions using the timeslice range 4–20. The contaminating amplitude in the R_{20} source smeared correlator clearly shows a zero at $r_0 \simeq 3.0$.

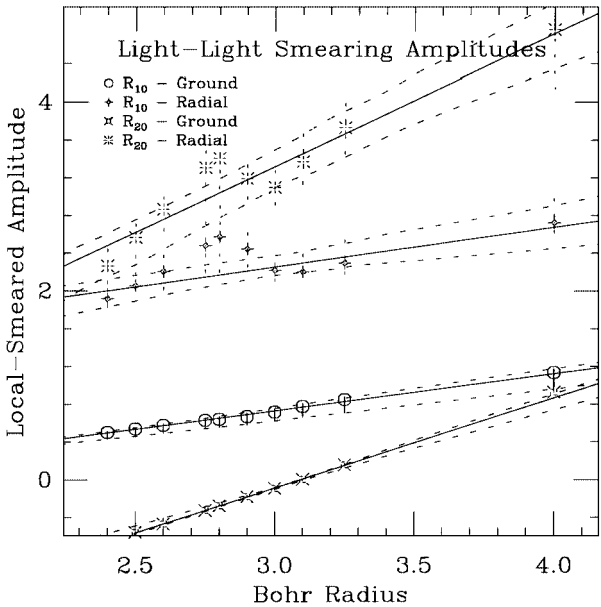

FIG. 9. Fitted amplitudes for light–light local source–sink smeared correlation functions using the timeslice range 4–20. The contaminating amplitude in the R_{20} sink smeared correlator clearly shows a zero at $r_0 \simeq 3.1$.

In fact, it should always be possible to orthogonalize the first radially excited smearing with respect to the physical ground state by tuning the Bohr radius parameter even when the physical states are not hydrogenic. One choice for the radius will not, however, simultaneously minimize the overlaps C_{10} and C_{01}. The better the ansatz for the smearing functions, the closer together we expect the optimal radii for the ground state and excited state correlators to lie. Where the ansatz is better, we also expect there to be less contamination from the higher excited states, since the physical wavefunctions are all mutually orthogonal.

In order to demonstrate the applicability of this smearing technique, a feasibility study was carried out on a small sample, with a large number of smearing radii, in the light–light, heavy–light, and heavy–heavy sectors.

IV. FEASIBILITY STUDY

We use the notation R_{nl} to denote smearing with the corresponding hydrogenic wavefunction with some Bohr radius. Fourteen quenched configurations of a $24^3 \times 48$ lattice at $\beta = 6.2$ were used with nonperturbatively $O(a)$ improved quarks (i.e., $C_{sw} = 1.61377$).

TABLE IX
Optimal Bohr Radii

System	Fitted Value	Choice
2300–2300	2.62 (2)	2.6
2300–3460	2.98 (2)	3.0
3460–3460	3.09 (1)	3.1

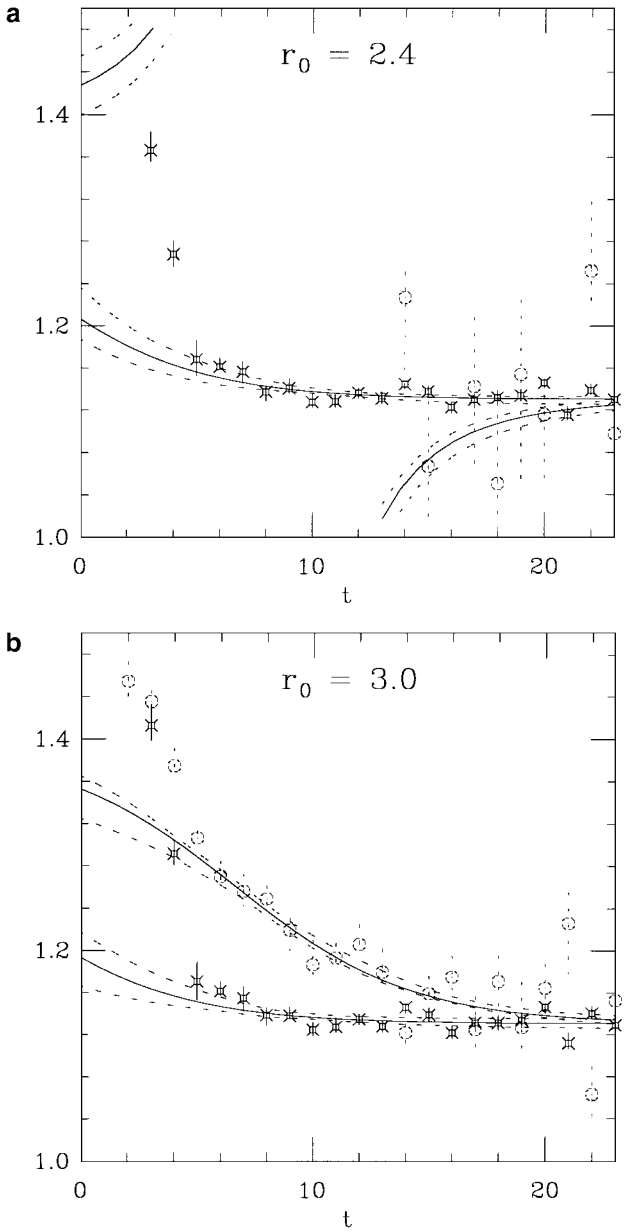

FIG. 10. R_{10}–R_{10} source and sink smeared quarkonium correlator (fancy squares), used in a double exponential fit with the R_{20} source, local sink correlator (circles) with Bohr radius $r_0 = 2.4, 3.0$.

Kappa values 0.13460 and 0.12300 were used, corresponding to quarks near the strange and charm masses, respectively. The lighter quark propagators had local sources, and both local and R_{10} sources were generated for the heavy propagator with Bohr radii of 2.4, 2.5, 2.6, 2.75, 2.8, 2.9, 3.0, 3.1, 3.25, 4.0, and 5.5 in lattice units. This allowed the smearing combinations in Table I to be generated for each Bohr radius. The correlation functions were analyzed using uncorrelated fits, because the small statistical sample caused the correlation matrix to be too noisy for reliable inversion in correlated fits. As such, the estimates of χ^2 are probably unreliable.

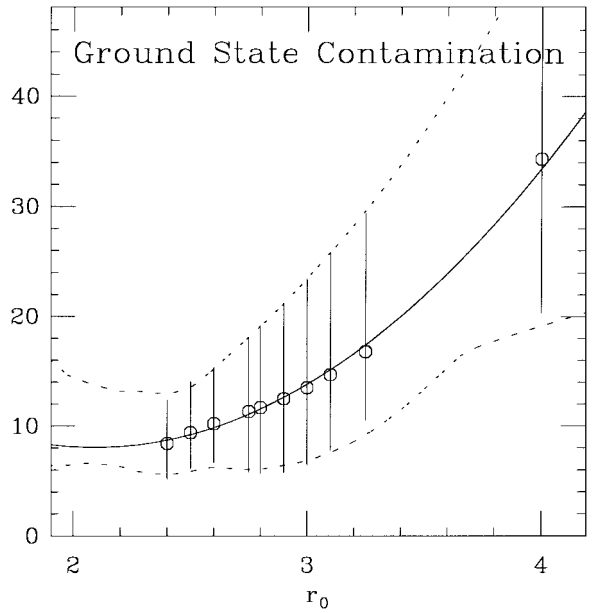

FIG. 11. Contaminating amplitude obtained from the R_{10}–R_{10} source and sink smeared quarkonium correlator. This smearing radius minimizing this amplitude lies in the region of 2.1(4).

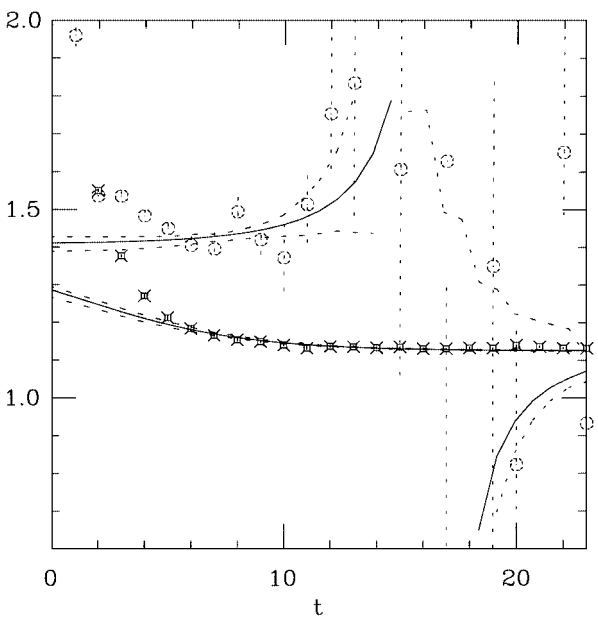

FIG. 12. Fit to the doubly R_{10} source smeared with local sink correlator (fancy squares) and the R_{20} source smeared with local sink correlator (circles) for the heavy–heavy meson. The quality of the plateau suggests that the use of double smearing is worthwhile for additional information on the ground state.

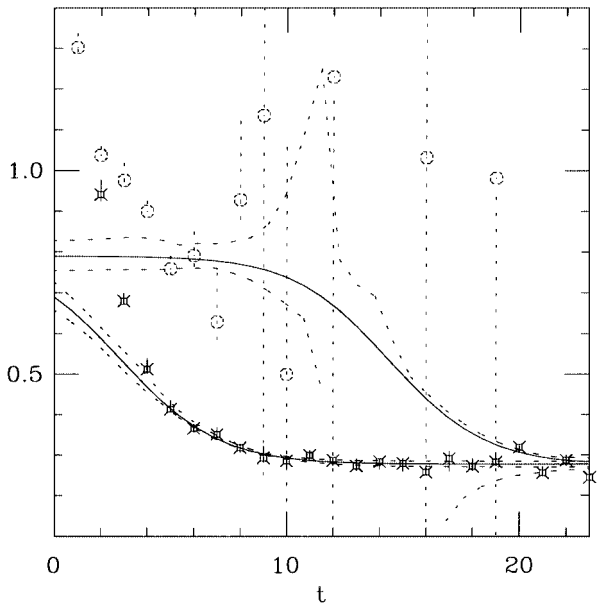

FIG. 13. Fit to the doubly R_{10} sink smeared with local source correlator (fancy squares) and the R_{20} sink smeared with local source correlator (circles) for the light–light meson.

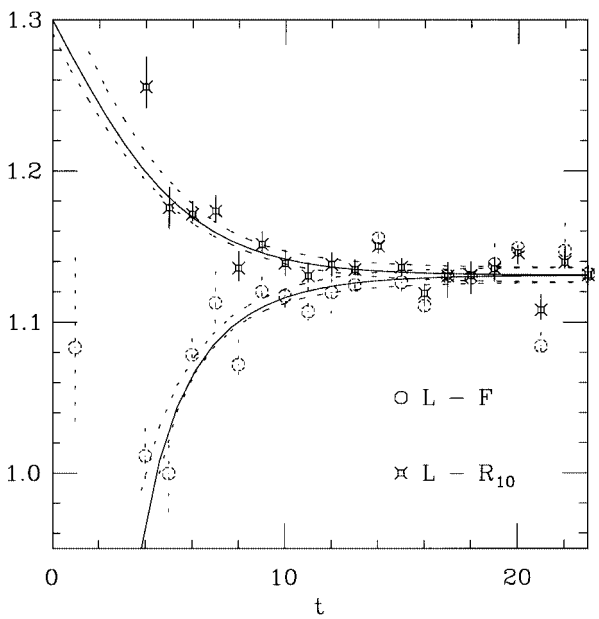

FIG. 14. Heavy–heavy fuzzed ($r = 6$) and R_{10} comparison. Both correlation functions are sink smeared with local sources on the same configurations. The lower statistical scatter our smearing technique is thought to be in part due to including a nonzero contribution from the local current.

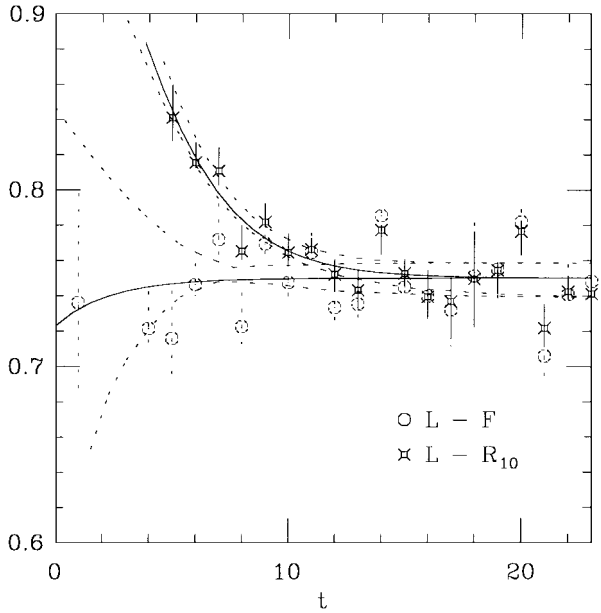

FIG. 15. Heavy–light fuzzed ($r = 6$) and R_{10} comparison. Both correlation functions are sink smeared with local sources on the same configurations.

Of primary interest is the simultaneous two exponential fit to the R_{10} and R_{20} source smeared–local sink correlation functions. These are used for the heavy–heavy and heavy–light mesonic states; however, in the case of light–light mesons source smearings were unavailable. We therefore substitute local source–sink smeared correlation functions in this case, which carry additional statistical noise but should yield identical results under the configuration average

We show the fitted effective masses for various Bohr radius for the heavy–heavy, heavy–light, and light–light sectors in Figs. 1 through 6.

The effective mass for the radially excited smearing demonstrates the expected transition in behavior, and appears to be forming a plateau for $r_0 = 2.6(3.0, 3.1)$ in the heavy–heavy (heavy–light, light–light) sector. While the formation of an excited state plateau is clearly strongly dependent on the selection of r_0 to within about 0.1 (this is possible to do using only one configuration by looking for vertical asymptote in the effective mass plot), we do not wish the fitted values to be dependent on the smearing. To investigate this, we study the stability of the fitted masses with the input parameters to the fitting procedure, namely the Bohr radius, and the timeslice range of the fit.

A. *Stability Analysis of Fitted Masses*

The fitted values for the ground state and excited state masses are given in Table II to Table V, and are found to be remarkably stable in the fit range typically agreeing within statistical error for all values of $t_{min} \geq 3$. The level of statistical error on the excited state mass is also particularly pleasing. The error on the excited light–light state is typically between only 5 and 10 times larger than that on the ground state.

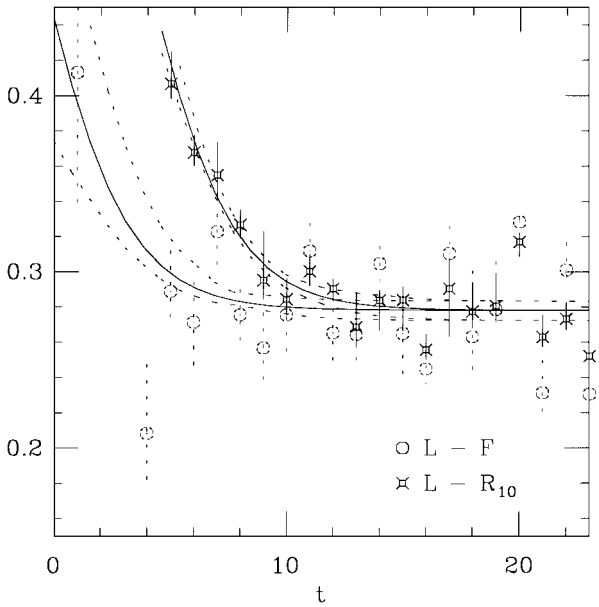

FIG. 16. Light–light fuzzed ($r = 8$) and R_{10} comparison. Both correlation functions are sink smeared with local sources on the same configurations.

In order to study the stability of the fits with respect to the chosen Bohr radius, the fitted mass values corresponding to $t_{min} = 4$ for all the simulated Bohr radii are tabulated in Tables VI, VII, and VIII. They are stable within the statistical error over almost the entire range of radii simulated.

B. *Selecting the Bohr Radius*

From inspection of the effective mass plots presented, we can see that the optimal values of the Bohr radius parameter (at least for the R_{20} correlator) were about 2.6 for the heavy–heavy state, 3.0 for the heavy–light, and 3.1 for the light–light. Using the discussion in Section III, we plot the fitted amplitudes of the local-smeared correlation functions versus Bohr radius, looking for the zero of the overlap of the R_{20} correlator with the ground state.

Figures 7–9 present the dependence of the four fitted amplitudes on the Bohr radius used in the heavy–heavy, heavy–light, and light–light systems, respectively. The linear fits are a good approximation, producing the optimal values for the smearing radii given in Table IX.

While the effective mass plots presented were on 14 configurations, it is clear that following the pole on the plot gave very accurate optimization of the Bohr radius, as demonstrated by later fits to the amplitudes. It was anticipated in Section III that, since our smearing function basis is not the physical one, the radius for minimal contamination of the ground state by the excited state would differ slightly from the radii which gave minimal contamination of the excited state. This is not apparent from the data presented in Figures 7–9, where there is no minimum of the R_{10}-excited state amplitude. We must bear in mind however that the contamination of the R_{10} correlator is measured at early times, whereas the contamination of the R_{20} correlator is found from its asymptotic time dependence, leaving the determination

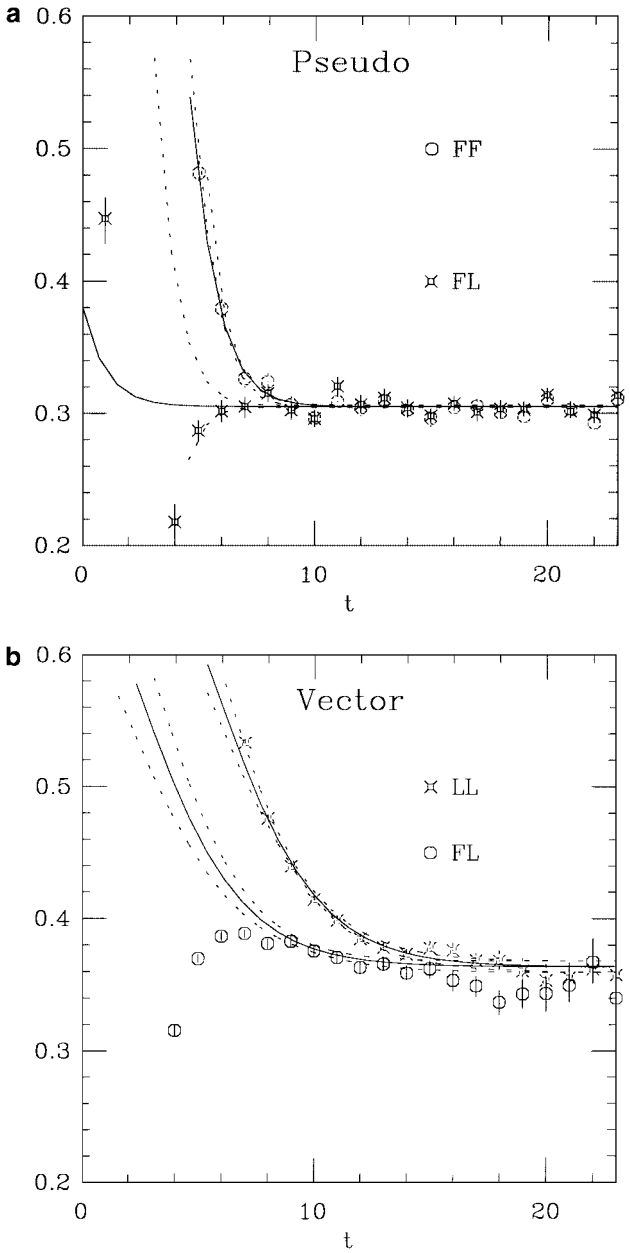

FIG. 17. Examples of approaches to fuzzed plateaux with high statistics. Opposing overlaps with the second and third excited states can cause nonmonotonic approaches. This is shown in the vector plot, where the open circles represent the fuzzed source, local sink state. The pseudoscalar plot shows a false plateau in the fuzzed–local correlation function, since the fuzzed–fuzzed correlator forms a plateau later we know that the early points in fuzzed–local correlator plateau *cannot* contain pure information about the ground state.

of the optimal Bohr radius from the R_{10} correlator much more subject to contamination from higher excited states. For this reason, it is dangerous to look only at the local–smeared amplitude, since cancelling contributions from the higher states can cause a seemingly flat effective mass.

Instead, we study the smeared–smeared correlators, which have positive definite contaminating contributions, and minimize the amplitude for the contamination of the R_{10}–R_{10} correlator. These correlation functions were only generated for the heavy–heavy combination, and Fig. 10 presents a sample fit to the pseudoscalar data. Here the contamination below timeslice 5 is apparent, as well as a weaker drift to the plateau beyond this point. It is this ultimate drift we must study. Figure 11 plots the fitted contaminating amplitude for this correlator versus radius; we expect from Section III a quadratic dependence on the smeared–smeared correlator. We obtain a minimizing radius of $r_0 = 2.1(4)$ with a quadratic fit.

C. *Use of Doubly Smeared Correlation Functions*

In this section I demonstrate that the signal obtained from doubly smeared correlators is useful. The double smearing is created by constructing the meson propagator from two propagators, each of which are smeared at the same end, while for the purposes of this demonstration, we use local operators at the other end. The double exponential fit to the double R_{10} and single R_{20} smeared correlation functions are presented in Figures 12 and 13 for the heavy–heavy and light–light systems, respectively. Clearly, this smearing combination, while not tailored for any particular state constitutes a valid signal that can be included in multichannel multi-exponential fits, which is always of use, especially for the p-states.

V. COMPARISON WITH FUZZING

In order to fairly compare the level of statistical error with traditional techniques, I present double exponential fits to the R_{10} sink and the fuzzed sink, both with the optimal radius in Figs. 14–16 for the heavy–heavy, heavy–light, and light–light systems, respectively, on the same set of local source propagators.

It can be seen that the statistical error from the R_{10} correlator is much reduced with respect to the fuzzed data. Admittedly, the fuzzed data does appear to plateau earlier, with a caveat however. The noise on the fuzzed data is such that there is quite possibly a "double approach" to the plateau because of contributions from more than one excited state, as seen in the large statistics fuzzed data at $\beta = 6.2$ in Fig. 17, so that with higher statistics the plateau may well not survive. It has also been found that the fuzzed–fuzzed combination tends to plateau after the fuzzed–local, indicating opposing contributions from excited states, and meaning that the plateau at early times is a misleading balance between contaminations of opposite sign (at least until after the fuzzed–fuzzed correlator has reached a plateau; c.f. Fig. 17).

VI. CONCLUSIONS

This smearing method provides, for the first time, a gauge invariant technique for inserting arbitrary radial wavefunctions in a smeared operator. So far, results have only been presented using hydrogenic wavefunctions, though in principle any form could be used. Excellent stability of fits to both the ground and radially excited states was demonstrated, and the level of statistical error was significantly smaller than traditional techiques on the same ensemble. Tuning the radius of the wavefunctions allowed a clear plateau for the radially excited state to be isolated. An understanding of the dependence of the fitted amplitudes on the radius of the smearing was obtained, which can be used to determine more accurately the optimal radius.

TABLE X
Comparison of 2S-1S Splittings with Experiment Using String Tension Scale

System	Lattice (MeV)	Experimental (MeV)
Light Pseudoscalar	1370 (50)	1170 (100) (π)
Light Vector	1250 (100)	700 (25) (ρ)
Heavy-Light Pseudoscalar	970 (60)	—
Heavy-Heavy Pseudoscalar	710 (60)	590 (J/ψ)

The feasibility study did not include a sufficient number of quark masses to extrapolate to the physical spectrum, however a rudimentary comparison of the $2S$–$1S$ splittings with experiment is made in Table X, and can be seen to be plausible. The main source of error, particularly in the light–light system, is expected to be finite volume effects, since the Bohr radius required suggests the extent of the wavefunction is significantly bigger than the lattice used.

Since the technique allows a free choice for the wavefunction, it would be interesting to try to find a better basis than the hydrogenic wavefunctions. Harmonic oscillator wavefunctions have been tried and found to be inferior to hydrogenic. Other possible options are numerically solving the Cornell potential and inserting the solution as the smearing function, as has been performed by the SESAM collaboration in the gauge fixed context [8], or alternatively measuring the wavefunction within a lattice calculation and reinserting this. It would be interesting to compute the R_{20} smeared correlators on a large volume for light quarks since we expect finite volume effects on the current volume.

ACKNOWLEDGMENTS

The work of this paper was carried out under the supervision of Richard Kenway, Ken Bowler, and Brian Pendleton, whom I thank for many useful conversations. I also thank Christine Davies for proofreading this work. The calculations were performed on the Cray T3D at the EPCC using UKQCD computer time. I acknowledge the support of EPSRC grant GR/K41663 and PPARC grant GR/K55745. The author was funded by the Carnegie Trust for the Universities of Scotland while this work was carried out at the University of Edinburgh, and is grateful for PPARC grant PP/CBA/62, and to the University of Glasgow for support while writing this paper.

REFERENCES

1. S. Gusken, U. Löw, K.-H. Mütter, R. Sommer, A. Patel, and K. Schilling, Nonsinglet axial vector couplings of the baryon octet in lattice QCD, *Phys. Lett.* **227**, 266 (1989).
2. C. Allton *et al.*, Gauge invariant smearing and matrix correlators using Wilson Fermions at Beta = 6.2, *Phys. Rev.* **D47**, 5128 (1993).
3. P. Lacock, A. McKerrell, C. Michael, I. M. Stopher, and P. W. Stephenson, Efficient hadronic operators in lattice gauge theory, *Phys. Rev.* **D51**, 6403 (1995).
4. V. Gribov, Problem of color confinement in nonabelian gauge theories, *Nucl. Phys.* **B139**, 1 (1978).
5. C. Parrinello, E. Marinari, and R. Ricci, Evidence for the existence of Gribov copies in Landau gauge lattice QCD, *Nucl. Phys.* **B362**, 487 (1991).
6. M. Alford, T. Klassen, and P. LePage, The D234 action for light quarks, *Nucl. Phys.* **B47** (Proc Suppl), 370 (1996).
7. C. Davies, K. Hornbostel, A. Langnau, G. P. Lepage, A. Lidsey, J. Shigemitsu, and J. Sloan, Precision upsilon spectroscopy from nonrelativistic lattice QCD, *Phys. Rev.* **D50**, 6963 (1994).
8. N. Eicker, T. Lippert, K. Schilling, A. Spitz, J. Fingberg, S. Gusken, H. Hoeber, and J. Viehoff, Improved upsilon spectrum with dynamical Wilson Fermions, *Phys. Rev.* **D57**, 4080 (1998).